Coupling of Nitrogen-Vacancy Centers to Photonic Crystal Cavities in Monocrystalline Diamond

Andrei Faraon,[1,2,*] Charles Santori,[1] Zhihong Huang,[1] Victor M. Acosta,[1] and Raymond G. Beausoleil[1]

[1]*Hewlett Packard Laboratories, 1501 Page Mill Road, Palo Alto, California 94304, USA*
[2]*California Institute of Technology, Department of Applied Physics and Material Science, 1200 East California Boulevard,
Pasadena, California 91125, USA*

The zero-phonon transition rate of a nitrogen-vacancy center is enhanced by a factor of ~ 70 by coupling to a photonic crystal resonator fabricated in monocrystalline diamond using standard semiconductor fabrication techniques. Photon correlation measurements on the spectrally filtered zero-phonon line show antibunching, a signature that the collected photoluminescence is emitted primarily by a single nitrogen-vacancy center. The linewidth of the coupled nitrogen-vacancy center and the spectral diffusion are characterized using high-resolution photoluminescence and photoluminescence excitation spectroscopy.

Nitrogen-vacancy (NV) centers in diamond represent one of the best test beds for future quantum photonic technologies [1,2], due to their outstanding properties as spin qubits [3] that can be coupled to optical photons [4]. Applications include quantum information [5] and electromagnetic field sensing [6–8]. For quantum information applications, multiple NV centers need to be interconnected. One approach relies on integrating NVs in photonic networks, where large-scale entanglement between NV centers is created using interference of identical photons at the zero-phonon line (ZPL) frequency. However, in bulk diamond the ZPL transition accounts for only a few percent of the NV emission. Here we report ~ 70-fold enhancement of the transition rate through the ZPL for a single NV coupled to a photonic crystal cavity in monocrystalline diamond. These cavities are fabricated using scalable semiconductor fabrication techniques and can be further coupled into photonic networks [2].

The spontaneous emission rate enhancement of a particular dipole transition i of an emitter coupled to a microresonator relative to the uniform dielectric medium of the resonator is enhanced by the factor $(\frac{\tau_0}{\tau_{\text{leak}}})_i + F_i$ [9], where $1/\tau_0$ is the emission rate in the uniform dielectric medium, $1/\tau_{\text{leak}}$ is the emission rate outside the cavity mode, and

$$F_i = F_{\text{cav}} \left| \frac{\vec{E}(\vec{r}_i) \cdot \vec{\mu}_i}{|\vec{E}_{\max}||\vec{\mu}_i|} \right|^2 \frac{1}{1 + 4Q^2(\frac{\lambda_i}{\lambda_{\text{cav}}} - 1)^2}, \quad (1)$$

where $\vec{\mu}_i$ is the dipole moment, $\vec{E}(\vec{r}_i)$ is the local electric field at the emitter location $\vec{r}_i$, λ_{cav} is the cavity wavelength, λ_i is the emitter wavelength, and $|\vec{E}_{\max}|$ is the maximum value of the electric field in the resonator. For the case where the dipole is resonant with the cavity and also ideally positioned and oriented with respect to the local electric field, $F_i = F_{\text{cav}}$, where

$$F_{\text{cav}} = \frac{3}{4\pi^2} \left(\frac{\lambda_{\text{cav}}}{n} \right)^3 \frac{Q}{V_{\text{mode}}}, \quad (2)$$

n is the refractive index, and $V_{\text{mode}} = [\int_V \epsilon(\vec{r})|\vec{E}(\vec{r})|^2 d^3\vec{r}]/\max[\epsilon(\vec{r})|\vec{E}(\vec{r})|^2]$ is the optical mode volume of the resonator, with $\epsilon(\vec{r})$ the electric permittivity at position $\vec{r}$.

From Eq. (2) it can be inferred that the highest enhancement is achieved using optical resonators with small mode volume and high quality factors. Several groups are currently pursuing microcavities of various geometries for this purpose (see Ref. [1] for a review). We previously reported coupling of the NV ZPL to the modes of a diamond microring resonator [10]. Compared to microrings, photonic crystal cavities provide confinement in a smaller mode volume and thus higher coupling rates. They can have mode volumes smaller than one cubic wavelength and the simulated quality factors can reach $Q = 1.3 \times 10^6$ [11,12]. Another advantage of photonic crystal cavities is better efficiency of coupling into free-space collection optics [13]. Photonic crystal cavities with quality factors up to 700 have been fabricated previously in single-crystal diamond and were coupled to silicon-vacancy color centers [14–16]. Hybrid systems involving photonic crystals fabricated in gallium phosphide have also been investigated for coupling to NV centers in diamond nanocrystals [17,18], but these NVs usually suffer from poor spectral properties.

A scanning electron microscope (SEM) image of a photonic crystal resonator similar to that used in the experiment is shown in Figs. 1(b)–1(d) (the actual device is not shown because SEM imaging can affect the charge state of the NV). The device was designed using the parameters reported in Ref. [12] and consists of a linear three-hole defect photonic crystal cavity fabricated in a triangular lattice with period $a = 218$ nm, hole radius $r = 0.29a \sim 63$ nm, and membrane thickness $h = 0.91a \sim 198$ nm (The device shown in Figs. 1(b)–1(d) has a photonic crystal with hole radius of 57 nm, smaller than the actual device). The three lateral holes are shifted outward by $d_1/a = 0.21$, $d_2/a = 0.02$, and $d_3/a = 0.20$ [see Fig. 1(a)]. Quality factors as high as $Q = 6000$ can be achieved with this design, while the mode volume is $V_{\text{mode}} \sim 0.88(\lambda_{\text{cav}}/n)^3$ ($\lambda_{\text{cav}} = 637$ nm, $n = 2.4$
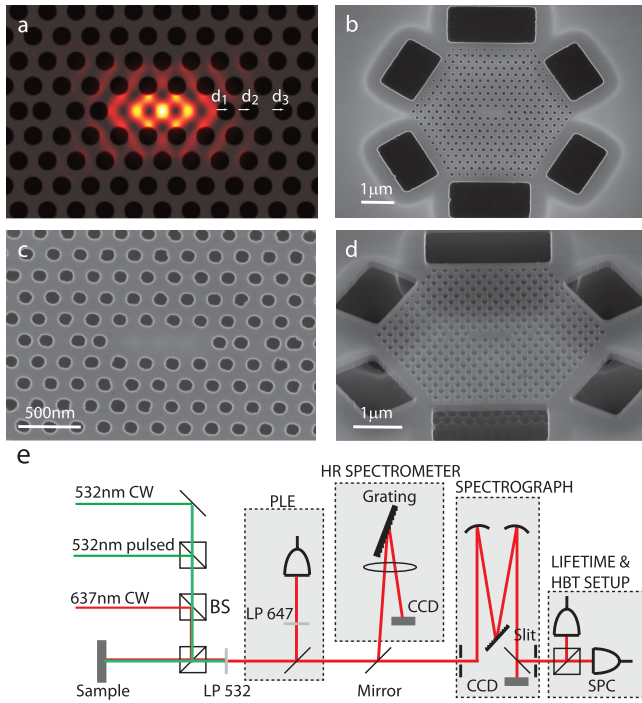
FIG. 1 (color).   (a) Color plot showing the electric field energy
density in the fundamental mode of a linear three-hole defect
cavity. The lateral three holes are shifted laterally by d_1, d_2, and
d_3 to increase the quality factor. (b)–(d) Scanning electron
microscope images of a photonic crystal cavity fabricated in
monocrystalline diamond. The black rectangles in (b) are open-
ings etched in the membrane to facilitate etching underneath the
membrane. The darker gray region around the openings indicates
the extent of the etched Si under the diamond. (e) Schematic of
the experimental setup. BS, beam splitter; LP, long pass filter;
SPC, single photon counter; HBT setup; HR, high resolution.

for diamond). The simulated profile of the electric field
energy density of the fundamental cavity mode is shown in
Fig. 1(a).

The fabrication recipe is based only on standard semicon-
ductor microfabrication techniques and is similar to the one
reported in Ref. [10] for microring resonators in single crystal
diamond. A ~200-nm thick diamond membrane was ob-
tained by thinning a 5-μm thick type IIa single-crystal
diamond membrane (Element Six, <1 ppm nitrogen, orien-
tation of the top face is 110) using reactive ion etching (RIE)
in an oxygen plasma. Prior to the etching process, the mem-
brane was mounted on a Si substrate. After the membrane
preparation, a silicon nitride (100 nm) layer was deposited on
top, and the photonic crystal device was patterned in this
layer using electron-beam lithography and RIE. Two more
etching steps were used to transfer the pattern from silicon
nitride to diamond and then remove the excess silicon nitride.
Finally, an isotropic dry etch removed the Si under the
photonic crystal, and the membrane at the device location
was left suspended [see Figs. 1(b)–1(d)].

The chip was placed in a continuous flow liquid helium
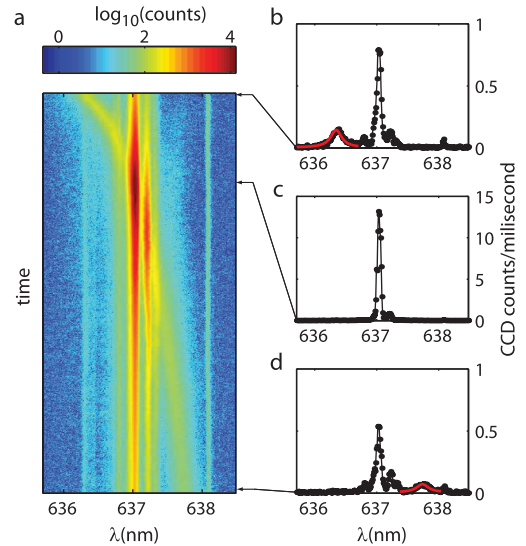cryostat (Janis UHV ST-500) and was characterized

FIG. 2 (color).   (a) Color plot showing the photoluminescence
spectra obtained while tuning the photonic crystal cavity over
the ZPL of nitrogen vacancy centers located in the cavity.
(b)–(d) Cross sections of the color plot. The cavity resonance
is marked with the red Lorentzian fit.

using a confocal microscope setup with ~1-μm spot size
[Fig. 1(e)]. The low temperature ($T < 10$ K) photolumi-
nescence (PL) spectra under continuous wave (cw) green
(532 nm) excitation are shown in Fig. 2. The ZPLs from a
few native NV centers that were incorporated accidently
during the crystal growth are visible at 637 nm (see
Ref. [10] for a discussion on inhomogeneous broadening),
together with the resonance of the cavity that is marked
by the red Lorentzian fit. We estimated a quality factor of
$Q \sim 3000$, about half of the value predicted by simulations
[12]. The discrepancy is caused by imperfections in the
fabrication process that causes nonuniformity in the hole
radius and rugged sidewalls that are visible in Fig. 1(c). To
observe coupling of the NVs to the cavity mode, the cavity
is tuned into resonance with the ZPL using a technique
where Xe gas is injected in the cryostat [19]. Strong
enhancement of the ZPL photoluminescence is observed
[Fig. 2(c)] when the cavity becomes resonant with the ZPL
of one of the NV centers, a signature of the spontaneous
emission rate enhancement.

Lifetime measurements were performed to determine
more accurately the coupling strength between the cavity
field and the ZPL transition. A pulsed green laser
(PicoQuant LDH-P-FA-530B, 532 nm, 100 ps pulse width,
100 μW average power) was used to excite the NV center,
and the PL emitted by the enhanced NV was filtered using
a monochromator (C bandwidth) and sent to a photon
counter (Perkin-Elmer SPCM). The lifetime is observed
to change from $\tau_{\text{off resonant}} = 13.7$ ns in the off-resonant
case [Fig. 3(a)] to $\tau_{\text{resonant}} = 4.0$ ns when the ZPL is on
resonance with the cavity [Fig. 3(b)]. The off-resonant
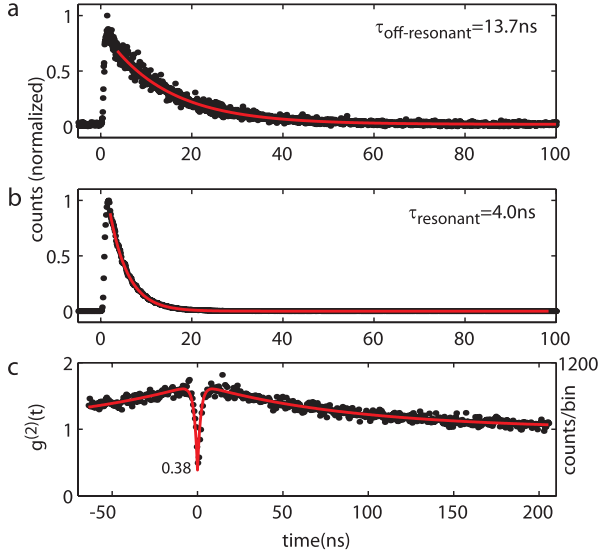lifetime is slightly larger than the usual value of

FIG. 3 (color). (a) Measurement of the lifetime ($\tau_0 = 13.7$ ns) of the NV center when not on resonance with the cavity. The measurement is performed on photoluminescence emitted in the ZPL. (b) Lifetime measurement when the NV is coupled to the cavity ($\tau_c = 4.0$ ns) (c) Second-order correlation [$g^2(\tau)$] measured on the zero-phonon line of the coupled NV. $g^2(0) = 0.38$ is estimated from the fit to the data (red line) that takes into account multiple decay paths. The bin size in the histogram is 1.1 ns.

$\tau_0 = 12$ ns generally observed in bulk diamond most likely due to the presence of the photonic band gap that decreases the optical density of states [20]. The zero-phonon spontaneous emission rate enhancement with respect to bulk can be derived using $F = (\tau_0/\tau_{\text{resonant}} - \tau_0/\tau_{\text{off-resonant}})/\xi_{\text{ZPL}}$, where ξ_{ZPL} is the zero-phonon spontaneous emission fraction in bulk diamond [10]. Considering that in bulk diamond $\xi_{\text{ZPL}} \sim 3\%$ of the light is emitted in the ZPL (from our own estimates on NV ensembles), the lifetime modification corresponds to a spontaneous emission rate enhancemet of $1 + F \sim 70$ (the value for F depends on ξ that varies in literature from 0.024 [21] and 0.04 [22]). The NV emits 70% of the photons in the ZPL. The measured enhancement is a factor of four lower than the maximum expected value of ~ 250 derived from Eq. (2) using the device parameters, which is likely due to suboptimal alignment of the dipole with the optical field. The orientation of the NV center within the cavity could be determined using an optically detected magnetic resonance method where the direction of the magnetic field is varied [23]. The location of the NV center could be detected with nanometer precision using stimulated emission depletion (STED) microscopy [24].

Emission lines from multiple NV centers are visible in the photoluminescence spectra in Fig. 2, but due to the relatively low density of NV centers, only very few (ideally one) are coupled to the mode of the cavity. One method to identify whether the PL comes from a single emitter is to perform a second-order correlation measurement using a Hanbury-Brown–Twiss (HBT) setup that consists of a

beam splitter and two single-photon counters positioned at the two output ports [see Fig. 1(e)]. Single photons (as emitted by a single NV) incident on the beam splitter can be directed only towards one of the counters, so the two counters cannot click at the same time. This can be tested by recording a time interval histogram for successive clicks on different counters.

In this way, second-order correlation measurements were performed on the photons emitted in the ZPL when an NV was on resonance with the cavity. A continuous-wave (380 μW, 532 nm) laser was used for excitation, and the collected light was spectrally filtered using the same setup as for the lifetime measurements. A total count rate of 30 000/s was obtained from the spectrally filtered ZPL. An antibunching dip in the coincidence rate was observed at zero time delay, as shown in Fig. 3(c). The dip extends over a few nanoseconds and sits within a positive ("bunched") peak that extends over a time scale of 100 ns. The behavior is typical for NV centers [25] and is caused by long-lived "shelving" states that do not emit light at the detection wavelength. The data were fitted using a formula for an emitter with three levels—a ground state, an excited state, and a shelving state [25]:

$$g^{(2)}(\tau) = 1 + c_1 e^{-\tau/\tau_1} + c_2 e^{-\tau/\tau_2}, \qquad (3)$$

where the coefficients c_1, c_2, τ_1, τ_2 depend on the pumping rate and the decay rates of the channels. The zero-time-delay autocorrelation was determined as $g^{(2)}(0) = 0.38$, with $\tau_1 = 1.88$ ns and $\tau_2 = 89$ ns (τ_1 is significantly shorter than the measured τ_{resonant} because the NV is driven close to saturation with a high pump rate). The value $g^{(2)}(0) = 0.38$ indicates that more than 75% of the photoluminescence comes from a single NV center well coupled to the photonic crystal resonator.

Enhancing the NV ZPL emission, as demonstrated above, is essential for increasing the success probability in quantum information schemes based on entangling NV centers via photon interference. An outstanding issue, however, is the spectral stability of NV centers which determines the entanglement fidelity in these schemes. We used high-resolution PL and photoluminescence excitation (PLE) spectroscopy to characterize the NV center coupled to the cavity. For the PLE measurements, a cw red laser diode was tuned to the NV ZPL transition for resonant excitation, and the PL emitted in the phonon sidebands was monitored while sweeping the laser frequency. The data are shown in Fig. 4(a), where two distinct spectral lines separated by ~ 20 GHz can be identified. The repeated scans, which are each followed by a 532-nm repump pulse, exhibit a combination of spectral diffusion behavior and a relatively broad width even from a single scan. The linewidths are approximately 4 GHz and 9 GHz for the left and right lines, or a factor of 100–225 greater than the cavity-modified lifetime limit of 40 MHz. For comparison, the best-quality synthetic diamond with less
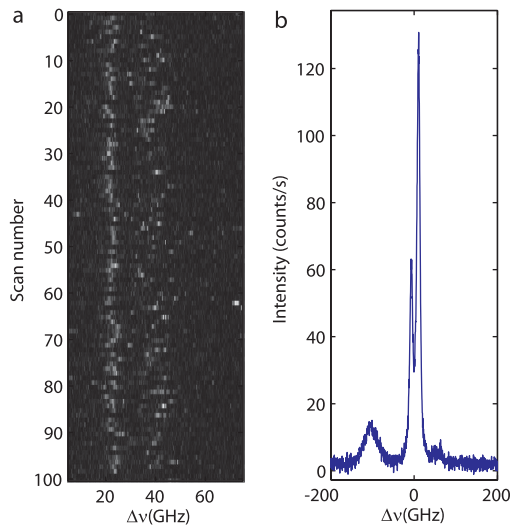
FIG. 4 (color). (a) Photoluminescence excitation measurement
at $T < 10$ K of the ZPL of the NV center coupled to the photonic
crystal cavity. (b) High-resolution photoluminescence measure-
ment of the same NV.

than 5 ppb nitrogen typically has spectral diffusion
linewidths of 100–200 MHz.

High-resolution PL spectroscopy was performed using a
home-built setup, based on a large echelle grating, provid-
ing 0.8 GHz resolution. Fig. 4(b) shows a photolumines-
cence spectrum taken when the NV is enhanced by the
cavity [the same conditions as in Fig. 2(c)]. As in the PLE
measurement, two distinct peaks are observed. The
FWHM of the main peak is approximately 8 GHz, com-
parable to that observed in the PLE measurement. The
presence of two peaks in the spectrum indicates either
the presence of two NV centers, with one being signifi-
cantly brighter than the other, or the strain-split $(X - Y)$
branches of the same NV center. The broader peak on the
left, presumably from another NV center, was outside of
the filter passband used for the lifetime and photon-
counting measurements described above.

In conclusion, we have demonstrated coupling of the
zero-phonon line of a single NV center to a photonic
crystal cavity fabricated in single-crystal diamond. The
spontaneous emission into the ZPL is enhanced by a factor
of ~ 70, which corresponds to $\sim 70\%$ of the photons being
emitted in the ZPL and into the cavity mode. The photonic
crystal platform allows for the possibility to dramatically
improve these results with better designs ($Q > 10^6$ is theo-
retically possible [11]) and improved fabrication tech-
niques. For example, with a mode volume of $\sim 1(\lambda/n)^3$
and a quality factor of $\sim 10^5$, the system can operate at the
onset of strong coupling regime, with more than 99% of
the emission into the ZPL. Using high-resolution spectros-
copy, we determined that the NV centers in this material
have a single-scan linewidth of a few GHz and a spectral
diffusion under 532 nm of several GHz, which is not

surprising for diamond of this quality (nitrogen concentra-
tion <1 ppm). However, the measured linewidth is two
orders of magnitude larger than the natural linewidth of
NV centers, a serious issue for quantum information appli-
cations, where linewidths smaller than the ground state spin
triplet splitting of 2.87 GHz are generally needed. For
sensing applications, enhancing the emission into the ZPL
increases the overall signal, thus enhancing the sensitivity.
However, the requirement to cool the device limits the range
of applications. Current and future effort is focused on
fabricating similar devices in diamond material with much
lower native nitrogen concentration (< 5 ppb), where the
measured linewidth is much closer to the natural linewidth
[26]. If such spectral stability can be maintained in micro-
fabricated structures, the resulting devices should enable
efficient implementation of remote entanglement between
NV centers via photon interference. In parallel, significant
effort is dedicated toward integrating these cavities with
electrodes used to stabilize the NV frequency against spec-
tral diffusion [27] and toward the development of complex
photonic networks as needed for quantum-information
devices for quantum chemistry [28] and factoring [29].

*andrei.faraon@hp.com
[1] I. Aharonovich, A. D. Greentree, and S. Prawer, Nature Photon. **5**, 397 (2011).
[2] J. L. O'Brien, A. Furusawa, and J. Vuckovic, Nature Photon. **3**, 687 (2009).
[3] G. Balasubramanian, P. Neumann, D. Twitchen, M. Markham, R. Kolesov, N. Mizuochi, J. Isoya, J. Achard, J. Beck, J. Tissler, V. Jacques, P. R. Hemmer, F. Jelezko, and J. Wrachtrup, Nature Mater. **8**, 383 (2009).
[4] E. Togan, Y. Chu, A. S. Trifonov, L. Jiang, J. Maze, L. Childress, M. V. G. Dutt, A. S. Sorensen, P. R. Hemmer, A. S. Zibrov, and M. D. Lukin, Nature (London) **466**, 730 (2010).
[5] L. I. Childress, J. M. Taylor, A. S. Sorensen, and M. D. Lukin, Phys. Rev. A **72**, 052330 (2005).
[6] C. L. Degen, Appl. Phys. Lett. **92**, 243111 (2008).
[7] J. M. Taylor, P. Cappellaro, L. Childress, L. Jiang, D. Budker, P. R. Hemmer, A. Yacoby, R. Walsworth, and M. D. Lukin, Nature Phys. **4**, 810 (2008).
[8] F. Dolde, H. Fedder, M. W. Doherty, T. Nobauer, F. Rempp, G. Balasubramanian, T. Wolf, F. Reinhard, L. C. L. Hollenberg, F. Jelezko, and J. Wrachtrup. Nature Phys. **7**, 459 (2011).
[9] E. M. Purcell. Phys. Rev. **69**, 681 (1946).
[10] A. Faraon, P. E. Barclay, C. Santori, K.-M. C. Fu, and R. G. Beausoleil, Nature Photon. **5**, 301 (2011).
[11] I. Bayn and J. Salzman, Opt. Express **16**, 4972 (2008).
[12] S. Tomljenovic-Hanic, M. J. Steel, C. M. de Sterke, and J. Salzman, Opt. Express **14**, 3556 (2006).

P H Y S I C A L R E V I E W L E T T E R S

[13] M. Toishi, D. Englund, A. Faraon, and J. Vučković, Opt. Express **17**, 14618 (2009).

[14] J. Riedrich-Moller, L. Kipfstuhl, C. Hepp, E. Neu, C. Pauly, F. Mucklich, A. Baur, M. Wandt, S. Wolff, M. Fischer, S. Gsell, M. Schreck, and C. Becher, Nature Nanotech. **7**, 69 (2011).

[15] T. M. Babinec, J. T. Choy, K. J. M. Smith, M. Khan, and M. Loncar, J. Vac. Sci. Technol. B **29**, 010601 (2011).

[16] I. Bayn, B. Meyler, A. Lahav, J. Salzman, R. Kalish, B. A. Fairchild, S. Prawer, M. Barth, O. Benson, T. Wolf, P. Siyushev, F. Jelezko, and J. Wrachtrup, Diam. Relat. Mater. **20**, 937 (2011).

[17] D. Englund, B. Shields, K. Rivoire, F. Hatami, J. Vuckovic, H. Park, and M. D. Lukin. Nano Lett. **10**, 3922 (2010).

[18] J. Wolters, A. W. Schell, G. Kewes, N. Nüsse, M. Schoengen, H. Döscher, T. Hannappel, B. Löchel, M. Barth, and O. Benson, Appl. Phys. Lett. **97**, 141108 (2010).

[19] S. Mosor, J. Hendrickson, B. C. Richards, J. Sweet, G. Khitrova, H. M. Gibbs, T. Yoshie, A. Scherer, O. B. Shchekin, and D. G. Deppe, Appl. Phys. Lett. **87**, 141105 (2005).

[20] D. Englund, D. Fattal, E. Waks, G. Solomon, B. Zhang, T. Nakaoka, Y. Arakawa, Y. Yamamoto, and J. Vučković, Phys. Rev. Lett. **95**, 013904 (2005).

[21] G. Davies, J. Phys. C **7**, 3797 (1974).

[22] P. Siyushev, V. Jacques, I. Aharonovich, F. Kaiser, T M. ller, L. Lombez, M. Atat re, S. Castelletto, S. Prawer, F. Jelezko, and J. Wrachtrup, New J. Phys. **11**, 113029 (2009).

[23] R. J. Epstein, F. M. Mendoza, Y. K. Kato, and D. D. Awschalom, Nature Phys. **1**, 94 (2005).

[24] E. Rittweger, K. Y. Han, S. E. Irvine, C. Eggeling, and S. W. Hell, Nature Photon. **3**, 144 (2009).

[25] C. Kurtsiefer, S. Mayer, P. Zarda, and H. Weinfurter, Phys. Rev. Lett. **85**, 290 (2000).

[26] K.-M. C. Fu, C. Santori, P. E. Barclay, L. J. Rogers, N. B. Manson, and R. G. Beausoleil, Phys. Rev. Lett. **103**, 256404 (2009).

[27] V. M. Acosta, C. Santori, A. Faraon, Z. Huang, K. Fu, A. Stacey, D. A. Simpson, S. Tomljenovic-Hanic, A D. Greentree, S. Prawer et al., Phys. Rev. Lett. **108**, 206401 (2012).

[28] B. P. Lanyon, J. D. Whitfield, G. G. Gillett, M. E. Goggin, M. P. Almeida, I. Kassal, J. D. Biamonte, M. Mohseni, B. J. Powell, M. Barbieri, A. Aspuru-Guzik, and A. G. White, Nature Chem. Biol. **2**, 106 (2010).

[29] M. A. Nielsen and I. L. Chuang, *Quantum Computation and Quantum Information* (Cambridge University Press, Cambridge, England, 2000).